

Experiments with a Holographic Radar Based on Software Defined Radio

Marcelo B. Perotoni  Marcos S. Vieira , and Rafael Bartolleti 

Abstract—The development of radar applications usually involves a complex set of different components, which can be costly and sometimes require careful handling. By concentrating most of the radar tasks into a software-defined radio, the hardware burden is alleviated, while the processing can be efficiently developed using open-source software suites. This article describes the development of a prototype radar based on a commercial software-defined radio, using only a few extra components. It operates under the holographic principle, where excitation is performed in single frequency, continuously transmitted. The tests have shown its potential applicability, carried out in an indoor environment, including through-the-wall detection.

Index Terms—Software-defined radio, radar, through-the-wall.

I. INTRODUCTION

Radars have been designed to operate in experimental and low-scale settings using affordable building blocks, such as off-the-shelf elements [1] and software-defined radios (SDRs), for a variety of applications. Commercial off-the-shelf components in radars have been used for hand gesture recognition [2], synthetic aperture radar (SAR) using drones at 24 GHz and 77 GHz [3], C-band through-wall imaging [4] and even avian [5] and insect [6] tracking. SDRs, in contrast to the use of building blocks such as low-noise amplifiers (LNAs), mixers, and filters, offer the versatility that comes from software-based reconfiguration. Frequency conversion, tuning, filtering, etc. are performed in baseband, i.e., downconverted in frequency by the SDR mixer, and can be dynamically changed with software without the need to change hardware components. Additionally, SDRs are self-contained, so there is no need for interconnecting cables, different DC levels to power subsystems, or shielding problems that arise when individual building blocks are used. In addition to the overall versatility, a not-so-apparent benefit of the SDRs is their ability to perform coherent detection. Even low-cost SDRs provide both in-phase (I) and quadrature (Q) components for the receiving stream. The complex information of the incoming wave is essential for imaging, which is performed using SAR. SAR is a technique that involves moving the antenna relative to the target, which enables geometric reconstruction (imaging) after the received echo [7]. A comprehensive justification and practical examples of the SDR use in radars is presented elsewhere [8]. In addition to SDRs and commercial elements, vector network analyzers (VNAs) can also be used for coherent

detection, but at the expense of a more fragile and costly instrument [9]–[12].

In particular, the concept of holographic radar, also known as continuous wave (CW) radar, can be defined as a radar that operates in the space domain [13], using a CW or single frequency [14]. It does not need to sweep a generator, such as frequency modulated continuous wave (FMCW) radar, which is commonly used to measure target speeds. The first mention of holographic radar in the open literature was made in 1969, using 34 GHz and photographic film to record the incoming data [15]. It basically correlates the complex response from the target with the spatial position, as in SAR, but using a single frequency [13].

This article describes experimental tests using a SDR-based radar, for the frequencies of 1 and 4 GHz, concentrating most functions inside the instrument. Section II describes the basics of two architectures, with the used hardware description. The software part of the radar is covered in Section III, and a practical indoor evaluation of the sensibility is presented in Section IV. Two indoor scenarios are tested in Section V, with through-wall experiments described in Section VI.

II. RADAR ARCHITECTURE

The two radar functions, transmitted (TX) and received (RX) can operate at the same time, case of the holographic type, or pulsed. The former requires at least two antennas, since both are operating at the same time. Regardless of the type, a receiver located at distance d from the target will receive the backscattered pulse after t_{echo} :

$$t_{echo} = 2d/c \quad (1)$$

where c is the speed of light. For a target 3 meters away, t_{echo} is 20 ns, which require very fast switching electronics in the case of a pulsed radar. Otherwise, the necessary resolution will not be achieved, and the response will be ambiguous. Ultra-fast switches that operate in the nanoseconds range with both low-cost and sufficient levels of isolation are not commercially available [16]. In case of targets that are further away, the receiver sensitivity is the limiting factor. This implies that larger transmitted amplitudes are needed to overcome the noise floor. On the other hand, radars might operate in full-duplex mode, where transmitting and receiving functions are simultaneous in the time domain. However, this means that there is a constant leak from the transmitting to the receiving antennas, which needs to be accounted for. Fig. 1 shows the main elements for a generic radar. Part of the RF generator is divided and fed into the mixer local oscillator (LO) port.

The signal reflected from the target, with lower amplitude, is input to the mixer RF port, resulting in a low-frequency signal output in the intermediate frequency (IF) port, which can be visualized in an oscilloscope, for example.

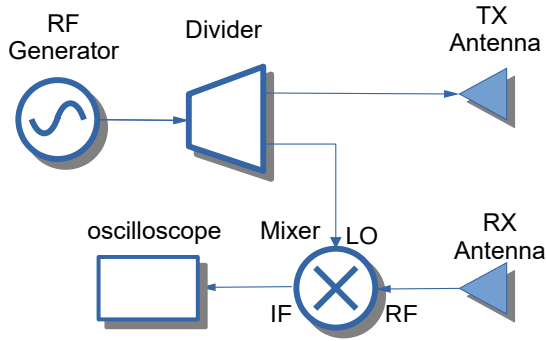


Fig. 1. Block diagram of a radar, operating in holographic mode.

The radar was based on the NI USRP B210, which can operate within the frequency range of 70 MHz to 6 GHz, with a maximum instantaneous bandwidth of 56 MHz. This particular SDR has relevant features for radar and imaging applications. It allows transmitting and receiving in full-duplex mode, unlike other lower-cost units, which only operate in half-duplex mode because they contain a single RF port. In addition, it has four RF ports, which can be configured in MIMO operation for both RX and TX. The four ports are divided in two sub-units, called Channels 0 and 1, so that they can operate within each channel either as TX or RX. Due to the internal architecture, another important feature is the coherent detection. This means that all ports are excited by the same local oscillator, so they are phase-locked, enabling phase measurements on the receiving signals. Fig. 2 shows the two tested architectures. One of the alternatives employs an external RF generator, which has part of its power sampled by a divider, attenuated by 30 dB and read by one of the receiving ports. This signal can be coherently compared to the other receiving port, thereby achieving amplitude and phase comparison. The advantage of having the added complexity of an external RF generator is that some SDRs have only two ports, operating as RX and TX, which makes it more complicated to extract a sample of the transmitted signal (case of the ADALM Pluto). An FMCW radar was reported using a similar B210 SDR, with two of its ports operating as receivers, and the transmitter employed a Pluto SDR, both synchronized by a cable connection [17]. Another subtle problem that arises when the SDR performs all the transmitter and receiver functions is the USB port overload. In case of using all four SDR ports, each supporting a 12-bit stream of 56 MHz, older generation USB ports might not be able to handle the data rate and run the risk of losing samples. The SDR only has therefore 2 ports set as RX and two as TX, one of the TX ports is unused but necessary due to a software or driver bug. The unused TX port is terminated with a 50 Ω load.

The main components of the radar are shown in Fig. 3, without the external generator. Two planar Log Periodic antennas (LPDA) were employed. The SDR is connected and power fed by a single USB connection to a computer.

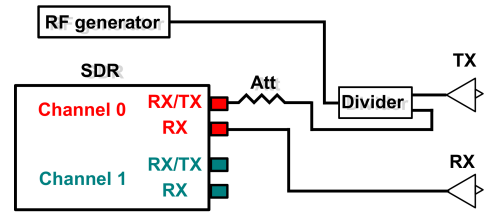
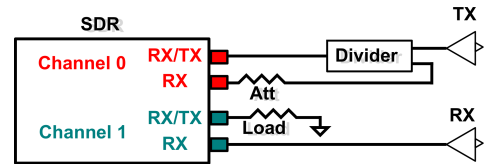


Fig. 2. Top, setup using only the SDR and bottom, using an external generator as exciter.

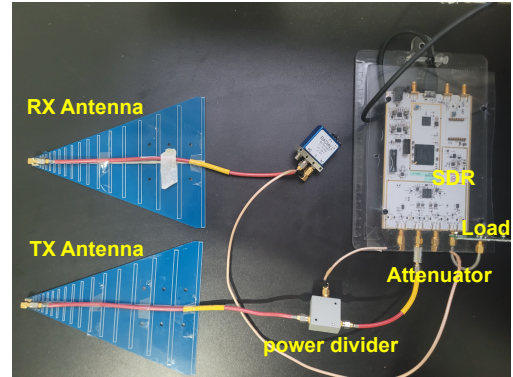


Fig. 3. Radar with the main components, using the internal RF USRP generator.

One of the most important parts of the SDR is the analog to digital converter (ADC) [18]. The SDR operational dynamic range is fundamentally defined by the ADC performance, which in turn is characterized by its number of bits. The B210's ADC has 12 bits (AD9361, a transceiver that operates in direct conversion), allowing a 74 dB theoretical dynamic range SNR_{dB} , given by Eq. 2, with N representing the number of bits. This represents a best-case scenario, and in this specific case, the B210 has a 24-dB advantage above the 8-bits, lower-cost HackRF One and RTL SDR.

$$SNR_{dB} = 1.76 + 6.02N[dB] \quad (2)$$

Since there are two similar antennas, if both are separated by a distance S their respective gain G , expressed in dB, can be estimated by means of the Friis Free space propagation formula:

$$G = 10 \log \left[\frac{4\pi S}{\lambda} \sqrt{\frac{P_{RX}}{P_{TX}}} \right] \quad (3)$$

where P_{TX} and P_{RX} are respectively the transmitted and received power and λ is the wavelength. Tests were performed in a non-ideal unshielded indoor environment. The broadside

shown. If the received amplitude is too faint, the LNA gain or the transmitter power (P_{TX}) can be increased. However, if both parameters are excessive, distortions will be seen in the displayed waveform. For protection, the transmitted power is always kept at moderate levels, not going beyond 60 % of its maximum amplitude (which is variable across the frequency range, measured 17 dBm for 1 GHz and 15.4 dBm for 4 GHz). The final program output is the magnitude and phase of the receiving wave, compared to the transmitter sample, the displayed waveforms help adjust power and amplification levels. This is shown in numeric fields as well as saved in binary files, to be processed later elsewhere. In the case of a static target, the complex ratio between the transmitted and received signals is also constant, ignoring noise fluctuations.

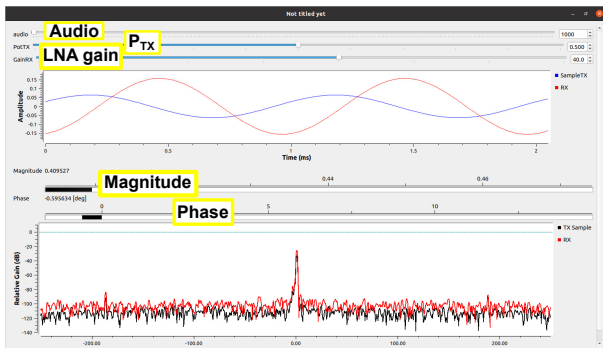


Fig. 6. Screenshot of the GNU Radio program.

Although GNU Radio has numerous functions for signal processing and visualization, it was observed that a lean flowgraph is preferable if a modest hardware is used. The tests were run in an 8 GB desktop running Ubuntu 22.04.

IV. SENSITIVITY EVALUATION

In order to evaluate the overall sensitivity, defined as the capacity of detecting the same target at different distances, a test was performed with the radar operating with the parameters shown in Table I.

TABLE I
RADAR PARAMETERS

F_{min} [GHz]	2
F_{max} [GHz]	3
P_{TX} [dBm]	0
N	21

Instead of a single frequency, N discrete frequency points are spread between F_{max} and F_{min} , as to explore other frequency ranges. Each one of the N discrete frequencies are transmitted, and the complex number relative to the echo is recorded (ratio between the transmitted and received samples). The operation differs from the usual FMCW radar, where the time delay between the transmitted and receiver frequency signals informs the target speed. It should be stressed also that since there is no pulsed operation, matched filtering techniques to increase the signal-to-noise ratio (SNR) are not applied. For

a better control on the absolute power level, an external generator was employed, set with output power P_{TX} . The generator also allows a higher amplitude, which helps visualize stronger echoes from the environment. The analyzed signal is the relative amplitude ratio between the backscattered waveform and the transmitted sample. Results were post-processed after extracted from the binary file. Regarding the scenario, Fig. 7 shows the radar placement in front of a metallic target, with the relevant parameters. The range distance d was varied, and the Inverse Fourier Transform (IFFT) together with Hermitian Processing was applied to the received data to recover the target distance, following details provided elsewhere [19], with the analogy that here the acquired relative complex amplitudes are related to scattering parameters in the reference. The test was performed indoors, so there is a large clutter and reflections from ground, ceiling and pieces of furniture present in the incoming data.

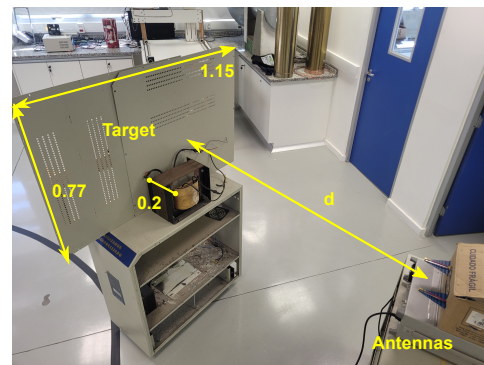


Fig. 7. Experimental setup to address the sensibility and functionality of the SDR radar.

After processing performed in Matlab, results are shown in Fig. 8 for two different distances, in absolute values. Given the acquired data in the frequency domain takes place over a finite bandwidth (between F_{min} and F_{max}), aliasing effects in radar imaging are avoided for distances in the range direction smaller than its maximum value d_{max} [7]:

$$d_{max} = c / [2\Delta f_{min}] \quad (4)$$

where Δf_{min} is the frequency sampling rate, 20 MHz for this present case. This results in a maximum range distance of 7.5 meters, so targets above this range appear aliased in wrong positions when the time-domain transform operation is performed. The environment contained objects in distances above this range, so they contributed to the observed clutter and noise in the final signals.

From the results, it is possible to see that the target position is seen on the expected pulse location. The line with absence of targets shows the influence of environment return echoes. As shown in the insert photo, there is a transformer placed in front of the plates, to hold the structure vertically stable, and its presence is shown in the pulse read previously to the largest amplitude echo.

V. TEST WITH MOVING TARGETS

Tests were performed using moving targets, the first with a metallic pendulum, a cylinder of 15.5 cm diameter and 33.5

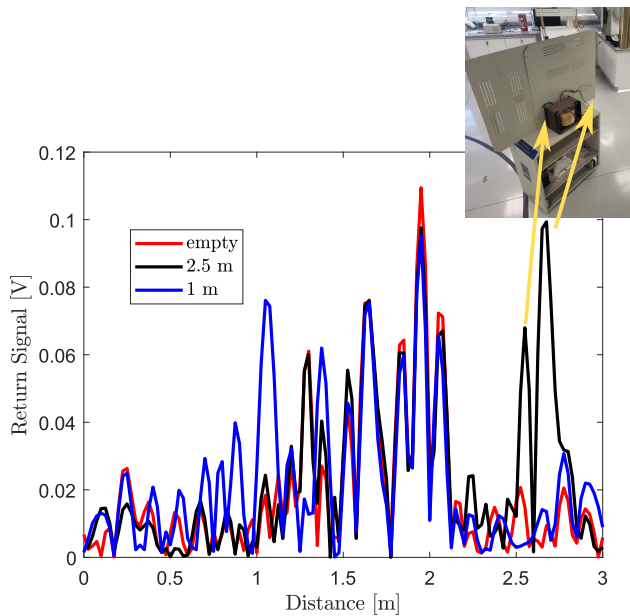


Fig. 8. Time-domain results after three different scenarios.

cm height, oscillating at approximately 1.8 meters from the radar, as shown in Fig. 9. The second test involved a moving adult target. Two evaluations were performed, with the radar operating in holographic mode (i.e., continuous frequency) at 1 GHz and 4 GHz. The internal generator of the SDR was used for this case, with its power set to half its maximum value, measured with a spectrum analyzer to be -30 dBm for both discrete frequencies.



Fig. 9. Scenario of the moving pendulum.

In terms of radar visibility, the parameter that enables the comparison between two targets is the target radar cross sections (RCS). Table II contains the RCS comparison between the cylinder and human body [20]. The pendulum had its RCS numerically evaluated by the Method of Moments (MoM) within the FEKO suite. A plane wave horizontal excitation was employed, orthogonal to the cylinder axial orientation, consistent with the experiment. The human body RCS is much larger for 1 GHz than that of the pendulum, a trend that is reversed for 4 GHz.

Results are shown in Fig. 10, normalized with respect to the maximum observed return amplitude - transmitted energy was considered constant throughout the test, with the steady

TABLE II
TARGET RCS [DBSM]

Target	1 GHz	4 GHz
Pendulum	-10.3	-1.6
Body	-4.2	-10

and moving pendulum. Approximately 1 minute of signal was acquired, so that the files do not increase too much in size (approximately 15 MB per minute). The pendulum movement was not mechanically controlled, so the differences in the observed waveforms are caused by the various trajectories and speeds by which the target moved. Nevertheless, results show that both frequencies captured the movement, with the 1 GHz showing a large SNR, considering the steady pendulum and the background response to be the noise.

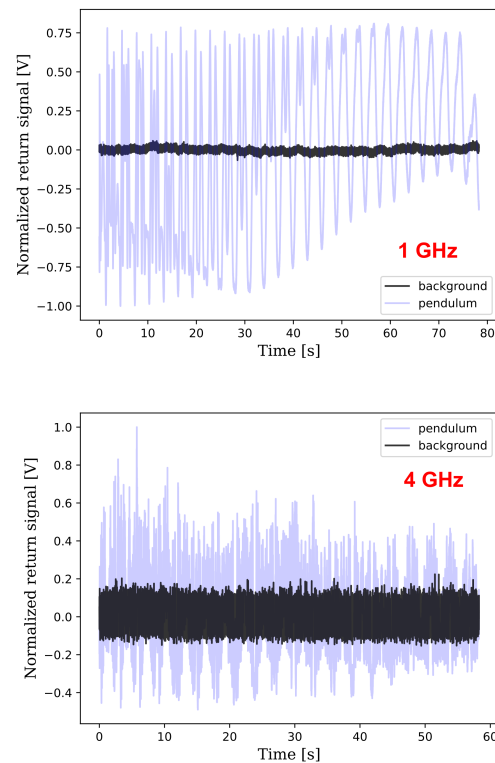


Fig. 10. Results for the pendulum, moving and steady, for two different frequencies.

The same test was performed for an adult, moving with normal pace and gait on the same indoor environment, for the two discrete frequencies. Movements were performed in different trajectories in relation to the antennas, comprising distances from 50 cm to 5 m. Results are presented in Fig. 11. Two different sets of movements were captured for each frequency, again limited to about one minute length. As in the former pendulum case, difference of the moving target against the background steady-pendulum is larger for the 1 GHz frequency.

A comparison among the SNR of the various scenarios is presented in Table III. The SNR was defined as:

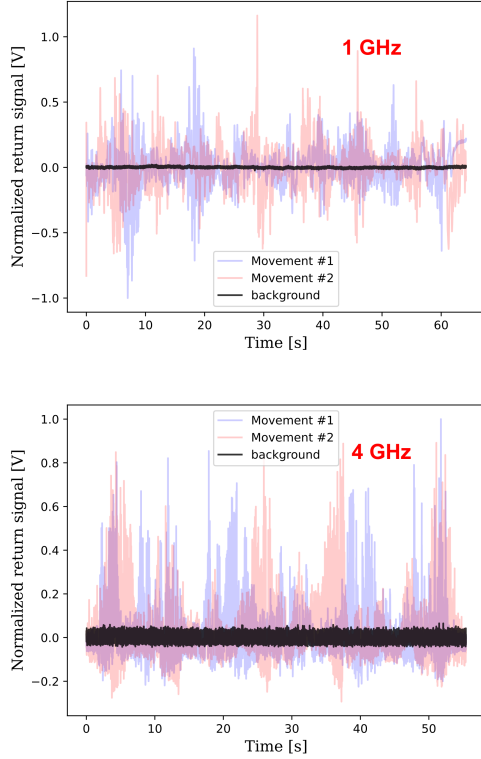


Fig. 11. Adult movement,captured for two different frequencies.

$$SNR = 20 \log [V_{signal}/V_{noise}] \tag{5}$$

where V_{signal} and V_{noise} are expressed in root-mean square (RMS). From the two scenarios, and considering the indoor environment, the frequency of 1 GHz generated better SNR figures.

TABLE III
SNR [DB]

Target	1 GHz	4 GHz
Pendulum	31.6	13.1
Body signal 1	40.5	17.3
Body signal 2	30.9	17.6

VI. THROUGH-WALL SCENARIO

Use of through-wall imaging has been subject of various applications, from homeland security to identifying victims under rubble [21]. Ultra wide-band signals (UWB) are usually employed for this, since using a large frequency range increases the possibility that some part of the signal will cross the barrier, bounce back, and arrive at the receiver with sufficient power [22]. Since the radar signal has to go through a solid barrier twice, the absorption it imposes plays a significant role. There is a trade-off between lower losses due to longer wavelengths and higher resolutions associated with shorter wavelengths. A common compromise that achieves good performance is the 1 to 3 GHz range, which unfortunately occupies a part of the spectrum that is occupied by several different communication services [21].

The measurement took place in an indoor environment, with the radar placed across a drywall barrier (approximately 16 cm thick). The antennas were placed horizontally 10 cm from the wall surface, not too close as to avoid a mismatch on the radiant elements. On the adjacent office, the same pendulum was moved at approximately 1.5 meter from the wall (Fig. 12).

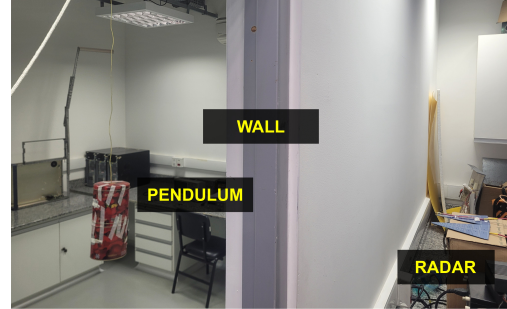


Fig. 12. Through-wall scenario.

Results are shown in Fig. 13, with the same power and software definitions as in the previous sections. It was noticed that the target visualized with 4 GHz had a smaller discrimination against ambient noise. Therefore, two different 60-seconds samples were taken with the pendulum for better comparison. By visual inspection, no pendulum movement is discernible in the 4-GHz waveform. The respective SNR for the two cases are summarized in Table IV. A performance difference between both discrete frequencies is seen in the plots as well as in the SNR results.

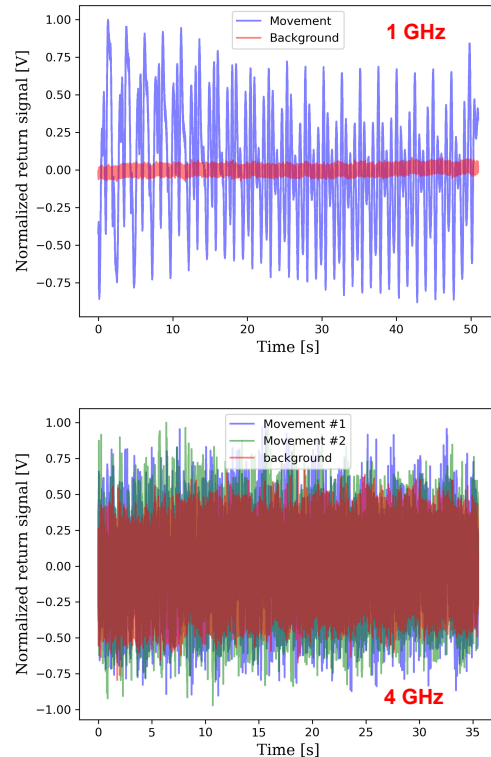


Fig. 13. Acquired response from the through-wall readings.

TABLE IV
SNR [dB]

Scenarios	1 GHz	4 GHz (I)	4 GHz (II)
SNR	26.5	2.92	3.0

The same hardware was used to evaluate the attenuation caused by the drywall barrier. A 69-cm linear distance was considered between the antennas, broadside alignment, with and without the wall obstruction. Table V shows the results, for four different frequencies. It can be seen that for this particular case, the 2 GHz signal has the smallest observed attenuation and both 1 and 4 GHz present similar levels of losses for the radar.

TABLE V
EXTRA ATTENUATION CAUSED BY THE DRYWALL
BARRIER

Frequency [1 GHz]	Attenuation [dB]
1	5.9
2	1.2
3	7.4
4	5.3

VII. CONCLUSIONS

This article described experiments with a SDR based holographic radar prototype. Two different architectures, one with an external RF generator and other without. Tests were performed in an indoor environment at low power levels. It was possible to visualize movements in distances around 5 to 10 meters, for a moving pendulum and a walking adult. Visualization of the target movement was also experienced behind a wall, with superior performance for the 1 GHz wave.

REFERENCES

- [1] G. Charvat, *Small and Short-Range Radar Systems*. CRC Press, 2014.
- [2] A. Sluyters, S. Lambot, and J. Vanderdonck, "Hand gesture recognition for an off-the-shelf radar by electromagnetic modeling and inversion," in *Proceedings of the 27th International Conference on intelligent user interfaces (IUI)*, 2022.
- [3] A. Bekar, M. Antoniou, and C. J. Baker, "High-resolution drone-borne SAR using off-the-shelf high-frequency radars," in *IEEE Radar Conference (RadarConf21)*, 2021.
- [4] H. Jeong and S. Kim, "Educational low-cost c-band fmcw radar system comprising commercial off-the-shelf components for indoor through-wall object detection," *Electronics*, vol. 10, pp. 1–11, 2021.
- [5] R. May, Y. Steinheim, P. Kvaløy, and F. Hanssen, "Performance test and verification of an off-the-shelf automated avian radar tracking system," *Ecology and Evolution*, vol. 7, pp. 5930–5938, 2017.
- [6] G. Storz and A. Lavrenko, "Compact low-cost fmcw harmonic radar for short range insect tracking," in *IEEE Radar Conference (RADAR)*, 2020.
- [7] C. Özdemir, *Inverse Synthetic Aperture Radar Imaging With MATLAB Algorithms*. Wiley, 2012.
- [8] J. M. Christiansen and G. E. Smith, "Development and calibration of a low-cost radar testbed based on the universal software radio peripheral," *IEEE Aerospace and Electronic Systems Magazine*, vol. 34, no. 12, pp. 50–60, 2019.
- [9] N. I. Avdievich, A. V. Nikulin, L. Ruhm, and A. W. Magill, "A 32-element loop/dipole hybrid array for human head imaging at 7 T," *Magn. Reson. Med.*, pp. 1–15, 2022.
- [10] J. Jehanzeb Burki, T. Ali, and S. Arshad, "Vector network analyzer (VNA) based synthetic aperture radar (SAR) imaging," in *Proceedings of the 16th International Multi Topic Conference (INMIC)*, 2013.

- [11] A. A. Pramudita, T. O. Praktika, and S. Jannah, "Radar modeling experiment using vector network analyzer," in *Proceedings of the International Symposium on Antennas and Propagation (ISAP)*, 2020.
- [12] J. Yu and M.-H. Ka, "Precision near-field reconstruction in the time domain via minimum entropy for ultra-high resolution radar imaging," *Remote Sens.*, vol. 9, no. 449, pp. 1–19, 2017.
- [13] L. Bossi, P. Falorni, and L. Capineri, "Versatile electronics for microwave holographic radar based on software defined radio technology," *Electronics*, vol. 11, pp. 1–16, 2022.
- [14] R. K. Amineh, M. Ravan, R. Sharma, and S. Baua, "Three-dimensional holographic imaging using single frequency microwave data," *Int. J. Antenn. Propag.*, vol. 2018, no. 6542518, pp. 1–15, 2018.
- [15] K. Iizuka, "Microwave hologram by photoengraving," *IEEE Proceedings*, vol. 57, no. 5, pp. 813–814, 1969.
- [16] M. R. P. Cerquera, J. D. C. Montaña, and I. Mondragón, *UAV for Landmine Detection Using SDR-Based GPR Technology*. Intech, 2017.
- [17] W. Feng, J. M. Friedt, and P. Wan, "SDR implemented ground-based interferometric radar for displacement measurement," *IEEE Trans. Instrum. Meas.*, vol. 70, pp. 1–18, 2021.
- [18] H. L. Hartnagel, R. Quay, U. L. Rohde, and R. M. (editors), *Fundamentals of RF and Microwave Techniques and Technologies*. Springer, 2023.
- [19] M. B. Perotoni, C. J. Bordin Jr., and K. M. G. dos Santos, "Conversion of scattering parameters to time-domain for imaging applications: Rules and examples," *Journal of Communication and Information Systems*, vol. 36, no. 1, pp. 1–7, 2021.
- [20] H. C. Kumawat and A. B. Raj, "Extraction of doppler signature of micro-to macro rotations/motions using continuous wave radar-assisted measurement system," *IET Sci., Meas. Technol.*, vol. 14, pp. 772–785, 2020.
- [21] M. G. Amin, *Through-the-wall radar imaging*. CRC Press, 2011.
- [22] S. Singh, Q. Liang, D. Chen, and L. Sheng, "Sense through wall human detection using UWB radar," *EURASIP Journal on Wireless Communications and Networking*, vol. 20, pp. 1–11, 2011.



Marcelo Bender Perotoni Electrical Engineering (UFRGS, 1995), MSc and PhD in Electrical Engineering (USP, 2001 and 2005). He is currently professor at UFABC, Santo Andre, and investigates the fields of RF, Microwave and EMC.



Marcos Stefanelli Vieira Electrical Engineering at UMC, Mogi das Cruzes, SP, 1996. MSc in Electrical Engineering from Univ. Presbiteriana Mackenzie, São Paulo, SP 2004 and PhD from Escola Politécnica da USP, São Paulo, SP, 2015. He is currently a professor at Univ. Presbiteriana Mackenzie.



Rafael Bartolleti Instrumentation, Automation and Robotics Engineering degree from UFABC, 2023, currently working towards a Masters degree in the UFABC Electrical Engineering program.